

Gauge-invariant observables and marginal deformations in open string field theory

Matěj Kudrna,¹ Toru Masuda,² Yuji Okawa,²
Martin Schnabl¹ and Kenichiro Yoshida³

¹*Institute of Physics AS CR
Na Slovance 2, Prague 8, Czech Republic*

²*Institute of Physics, The University of Tokyo
3-8-1 Komaba, Meguro-ku, Tokyo 153-8902, Japan*

³*Ministry of Internal Affairs and Communications
2-1-2 Kasumigaseki, Chiyoda-ku, Tokyo 100-8926, Japan*

matej.kudrna@email.cz, masudatoru@gmail.com, okawa@hep1.c.u-tokyo.ac.jp,
schnabl.martin@gmail.com, ken16.yoshida@gmail.com

Abstract

The level-truncation analysis of open string field theory for a class of periodic marginal deformations indicates that a branch of solutions in Siegel gauge exists only for a finite range of values of the marginal field. The periodicity in the deformation parameter is thus obscure. We use the relation between gauge-invariant observables and the closed string tadpole on a disk conjectured by Ellwood to construct a map between the deformation parameter of the boundary conformal field theory and the parameter labeling classical solutions of open string field theory. We evaluate the gauge-invariant observables for the numerical solutions in Siegel gauge up to level 12 and find that our results qualitatively agree with the analysis by Sen using the energy-momentum tensor and are consistent with the picture that the finite range of the branch covers one fundamental domain of the periodic moduli space.

1 Introduction

String field theory can potentially be a background-independent formulation of string theory. The current construction of string field theory, however, requires a choice of a consistent background, and different backgrounds are expected to be described by classical solutions of the theory based on the original background we chose.

Thus the first step to address the problem of background independence in string field theory is the construction of classical solutions. There has been remarkable progress in constructing analytic solutions in open string field theory [1] since the first construction of an analytic solution for tachyon condensation by one of the authors [2]. In particular, analytic solutions for marginal deformations of boundary conformal field theory have been constructed and intensively studied [3]–[21]. A systematic procedure to construct analytic solutions for marginal deformations to all orders in the deformation parameter has been presented in [12, 13]. On the other hand, there has been a puzzle associated with marginal deformations in the level-truncation analysis in Siegel gauge carried out in [22], where the deformation parameter was treated nonperturbatively. This is the problem we discuss in this paper. Let us first explain the setup and describe the puzzle.

When open bosonic string theory on a D25-brane is compactified on a circle of the self-dual radius $\sqrt{\alpha'}$, there are three marginal operators in the boundary conformal field theory (CFT) describing the compactified direction. The three operators are given by

$$V_1(t) \equiv \sqrt{2} : \cos \frac{X(t)}{\sqrt{\alpha'}} :, \quad V_2(t) \equiv \sqrt{2} : \sin \frac{X(t)}{\sqrt{\alpha'}} :, \quad V_3(t) \equiv \frac{i}{\sqrt{2\alpha'}} \partial_t X(t), \quad (1.1)$$

where $X(t)$ is the coordinate of the compactified direction. The marginal deformation by the operator V_3 corresponds to turning on a constant mode of the gauge field on the D-brane and is exactly marginal. Since the direction of the coordinate X is compactified, the one-dimensional moduli space of this deformation is periodic. These three operators are related by the enhanced $SU(2)$ symmetry at the self-dual radius, and so the marginal deformations by the other two operators V_1 and V_2 are also exactly marginal and the moduli space for each deformation is periodic. It is known that the deformation by the operator V_1 changes the original Neumann boundary condition to a Dirichlet boundary condition at a special point of the moduli space. In other words, the original D25-brane is deformed to a D24-brane by this marginal deformation.

We thus expect that the equations of motion of open string field theory formulated around a D25-brane compactified on the self-dual radius have a one-parameter family of solutions associated with each of the three marginal deformations, and the moduli space is periodic for each case. In [22] Sen and Zwiebach constructed solutions using level truncation in Siegel gauge. They computed the effective potential of the massless mode associated with the marginal deformation by solving the equations of motion for other fields. They found that the effective

potential is approximately flat and becomes flatter as the level of the approximation is increased, which is in accord with the expectation that we have a one-parameter family of solutions. However, they also found that the branch of the effective potential is truncated at a finite distance from the origin. The effective potential does not exist beyond that point, and this result seems stable as the truncation level is increased. It has been a long-standing problem to understand the nature of this phenomenon. First of all, the periodicity in the moduli space is obscure. In particular, it is important to know whether or not the point of the moduli space corresponding to a Dirichlet boundary condition in the case of the deformation by V_1 is within the branch.

In order to investigate this problem it is helpful to construct a map between the deformation parameter λ_{BCFT} of boundary CFT and the parameter λ_{SFT} labeling solutions of open string field theory. However, this has in general been a difficult problem. In [22] Sen and Zwiebach attempted to obtain information on the map in the case of the deformation associated with V_1 by slightly increasing the radius R of the compactification. The marginal deformation becomes a relevant deformation and the effective potential develops a local minimum corresponding to tachyon condensation. They used the location of the local minimum to identify the point of the moduli space corresponding to a Dirichlet boundary condition. However, the extrapolation to the self-dual radius $R \rightarrow \sqrt{\alpha'}$ is not smooth, and they were not able to obtain a definite conclusion.

Later Sen developed a different method to construct a map between λ_{BCFT} and λ_{SFT} in [23]. It is based on the energy-momentum tensor in spacetime. Its dependence on λ_{BCFT} can be calculated from the boundary state. Its dependence on λ_{SFT} was calculated from the dependence of the effective potential on the compactification radius R . The two results were combined and a map between λ_{BCFT} and λ_{SFT} was constructed based on numerical results by level truncation up to level 4.¹ In order to use this method, however, it is necessary to calculate the dependence of the effective potential on the compactification radius R . Furthermore, this method cannot be used for arbitrary marginal deformations. For instance, it cannot be used directly for the marginal deformation by V_3 because the relevant component of the energy-momentum tensor does not depend on the deformation parameter, although we can use the $SU(2)$ symmetry to convert the result for V_1 into that for V_3 .

In this paper we present a new approach to the construction of a map between the deformation parameter λ_{BCFT} of boundary CFT and the parameter λ_{SFT} labeling solutions of open string field theory for marginal deformations. It is based on a relation between gauge-invariant observables discovered in [25, 26] and the closed string tadpole on a disk conjectured by Ellwood [27]. If the closed string tadpole depends on the marginal deformation of boundary CFT, we can construct a map between λ_{BCFT} and λ_{SFT} by calculating the gauge-invariant observ-

¹ The analysis was extended to higher levels by André Kurs in his Senior Thesis at Princeton University [24].

able for the solutions of open string field theory. This method can in principle be used for any marginal deformation if there is a closed string tadpole which depends on the deformation parameter. Furthermore, the calculation on the string field theory side is much simpler than that of the method in [23]. The gauge-invariant observables depend linearly on the open string field and can be calculated by contracting the open string field and the identity state with an additional insertion of an on-shell closed string vertex operator.

The paper is organized as follows. In section 2 we briefly review the construction of the solutions for marginal deformations by Sen and Zwiebach in level truncation. In section 3 we apply the conjecture by Ellwood to the solutions for marginal deformations and explain how one can relate the parameter of the solutions in open string field theory with that of the corresponding boundary CFT. In section 4 we illustrate our computation using level truncation up to level 4. In section 5 we summarize our main numerical results for solutions with various values of λ_{SFT} obtained up to level 12. Our results are consistent with the picture that the finite range of the branch covers just one fundamental domain of the periodic moduli space. Further supporting tables and plots are presented in appendix A.

2 Marginal deformations in Siegel gauge

In this section we briefly review the result by Sen and Zwiebach in [22] for marginal deformations in open string field theory using level truncation. We consider open string field theory for a D25-brane in a 26-dimensional flat spacetime with one of the spatial directions compactified on a circle of the self-dual radius and the marginal deformation generated by $V_1(t)$.

The important features can already be seen at level 1. The string field truncated to level 1 is given by

$$t_0 c_1|0\rangle + t_1 : \cos \frac{X(0)}{\sqrt{\alpha'}} : c_1|0\rangle, \quad (2.1)$$

and the potential for the modes t_0 and t_1 with the normalization used in [22] is

$$V(t_0, t_1) = -\frac{1}{2} t_0^2 + \frac{27\sqrt{3}}{64} t_0^3 + \frac{3\sqrt{3}}{8} t_0 t_1^2. \quad (2.2)$$

Let us derive the effective potential for t_1 by solving the equation of motion for t_0 . Since the equation of motion for t_0 is a quadratic equation, there are two solutions:

$$t_0^M = \frac{4}{81\sqrt{3}} \left(-\sqrt{64 - \frac{729}{2} t_1^2} + 8 \right), \quad t_0^V = \frac{4}{81\sqrt{3}} \left(\sqrt{64 - \frac{729}{2} t_1^2} + 8 \right). \quad (2.3)$$

The superscript M denotes the *marginal* branch. The solution t_0^M vanishes as $t_1 \rightarrow 0$ so that this branch is associated with the marginal deformation. The superscript V denotes the

vacuum branch. The solution t_0^V is associated with the branch connected to the tachyon vacuum solution. We can see from these expressions that we do not have real solutions when

$$64 - \frac{729}{2} t_1^2 < 0. \quad (2.4)$$

The critical values $\pm \bar{t}_1$ for t_1 are thus given by

$$\bar{t}_1 = \frac{8\sqrt{2}}{27} \simeq 0.419. \quad (2.5)$$

The two branches meet at these critical values. Since the effective potential is even with respect to t_1 , from now on we focus our attention on the region $t_1 \geq 0$.

Corresponding to the two solutions t_0^M and t_0^V , there are two branches for the effective potential. By substituting t_0^M and t_0^V to $V(t_0, t_1)$, we obtain

$$\begin{aligned} V^M(t_1) &= \frac{2}{59049} \left(-512 + 4374 t_1^2 + \left(64 - \frac{729}{2} t_1^2 \right)^{\frac{3}{2}} \right) = \frac{27}{128} t_1^4 + \frac{6561}{32768} t_1^6 + \mathcal{O}(t_1^8), \\ V^V(t_1) &= \frac{2}{59049} \left(-512 + 4374 t_1^2 - \left(64 - \frac{729}{2} t_1^2 \right)^{\frac{3}{2}} \right) = -\frac{2048}{59049} + \frac{8}{27} t_1^2 + \mathcal{O}(t_1^4). \end{aligned} \quad (2.6)$$

The two branches $V^M(t_1)$ and $V^V(t_1)$ of the effective potential are shown in figure 1.

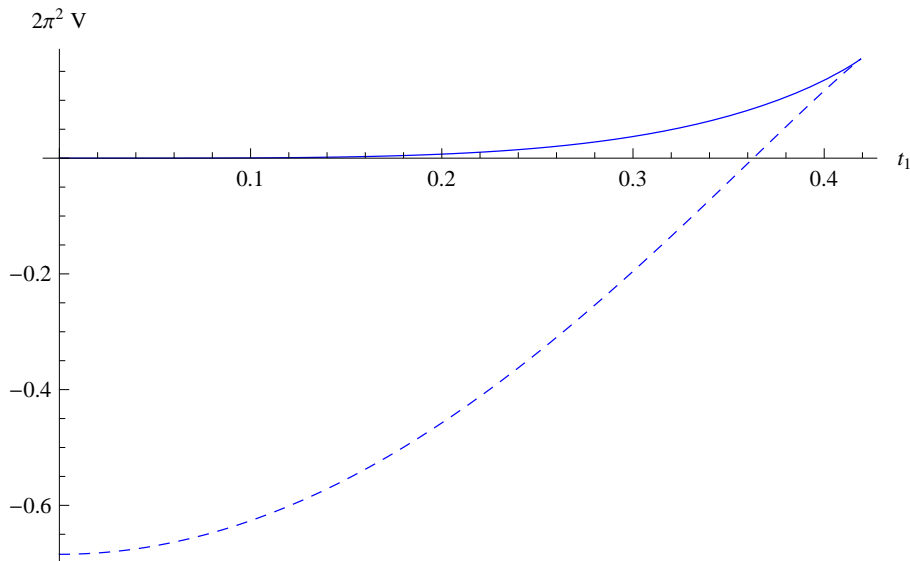


Figure 1: The two branches of the effective potential for t_1 at level 1. The solid line is for $2\pi^2 V^M(t_1)$ and the dashed line is for $2\pi^2 V^V(t_1)$.

We expect an exactly flat potential for the marginal branch because the deformation by $V_1(t)$ is known to be exactly marginal. The potential $V^M(t_1)$ at level 1 is not exactly flat, but this is considered to be an artifact of level truncation. The higher-order analysis in level

truncation shows that the effective potential for t_1 on the marginal branch becomes flatter as the truncation level is increased, as expected. See figure 2.² It has also been shown analytically that the coefficient in front of t_1^4 in $V^M(t_1)$ vanishes in the limit where the truncation level becomes infinite [28]. In this deformation, we can therefore use t_1 as the label λ_{SFT} of approximate numerical solutions in level truncation.

On the other hand, the existence of the critical value of t_1 does not seem to be an artifact of level truncation. The results at higher orders in figure 2 show that the critical value persists and the position of the critical value does not move significantly as the truncation level is increased. The analysis using level truncation thus indicates that the effective potential $V^M(t_1)$ on the marginal branch in Siegel gauge becomes exactly flat and terminates at a finite critical value in the limit where the truncation level becomes infinite.

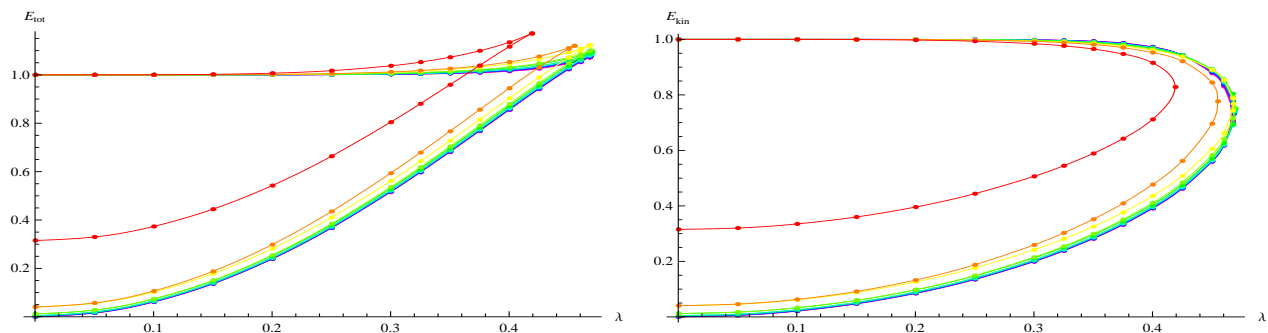


Figure 2: The energy density of the marginal and vacuum branches computed from the full action (the left graph) and from the kinetic term (the right graph). We have chosen t_1 as the parameter λ of the branches. The energy density is measured from the tachyon vacuum and normalized by the D25-brane tension. In this and other figures, the colors follow the spectrum: higher level results are depicted using shorter wavelength colors. For explicit color coding, see figure 15.

3 Gauge-invariant observables and the closed string tadpole

In [27] Ellwood conjectured a relation between gauge-invariant observables of open string field theory discovered in [25, 26] and the closed string tadpole on a disk. The gauge-invariant observable $W(\phi, \mathcal{V})$ for an open string state ϕ and an on-shell closed string vertex operator \mathcal{V} is defined by the following correlation function on the upper half-plane:

$$W(\phi, \mathcal{V}) = \langle \mathcal{V}(i) f_I \circ \phi(0) \rangle_{\text{UHP}}. \quad (3.1)$$

²The difference between the energy density E_{tot} computed from the full action and the energy density E_{kin} computed from the kinetic term is proportional to t_1 times the equation of motion for t_1 .

Here $\phi(0)$ is the operator corresponding to the state ϕ in the state-operator correspondence and we denote by $f_I \circ \phi(0)$ the conformal transformation of $\phi(0)$ under the map $f_I(\xi)$ associated with the identity state:

$$f_I(\xi) = \frac{2\xi}{1-\xi^2}. \quad (3.2)$$

The closed string tadpole on a unit disk defined in [27] is

$$\mathcal{A}^{\text{disk}}(\mathcal{V}) = -\frac{e^{-i\theta}}{2\pi i} \langle \mathcal{V}(0) c(e^{i\theta}) \rangle_{\text{disk}}. \quad (3.3)$$

This should be independent of θ . The unit disk with a complex coordinate w can be mapped to the upper half-plane of z by the following conformal transformation:

$$z = i \frac{1-w}{1+w}. \quad (3.4)$$

The correlation function on a unit disk in (3.3) can be mapped under this conformal transformation to

$$\mathcal{A}^{\text{disk}}(\mathcal{V}) = -\frac{1}{\pi} \frac{1}{1+t^2} \langle \mathcal{V}(i) c(t) \rangle_{\text{UHP}} \quad \text{with} \quad t = \tan \frac{\theta}{2}. \quad (3.5)$$

It is easy to confirm that $\mathcal{A}^{\text{disk}}(\mathcal{V})$ is independent of t when the ghost part of \mathcal{V} is $c\tilde{c}$. Ellwood conjectured the following relation:

$$W(\Psi, \mathcal{V}) = \mathcal{A}_{\Psi}^{\text{disk}}(\mathcal{V}) - \mathcal{A}_0^{\text{disk}}(\mathcal{V}), \quad (3.6)$$

where $\mathcal{A}_0^{\text{disk}}$ is the closed string tadpole with the original boundary condition and $\mathcal{A}_{\Psi}^{\text{disk}}$ is the closed string tadpole with the boundary condition corresponding to the classical solution Ψ . If the boundary CFT has marginal deformations labeled by λ_{BCFT} , we expect that the equation of motion of open string field theory has a one-parameter family of solutions labeled by λ_{SFT} . The left-hand side of (3.6) is a function of λ_{SFT} . The closed string tadpole appearing on the right-hand side of (3.6) is a function of λ_{BCFT} . We can thus obtain a map between λ_{BCFT} and λ_{SFT} from the conjectured relation (3.6).

We consider the marginal deformation by the cosine potential $V_1(t)$. We have to choose a closed string vertex operator \mathcal{V} such that the one-point function $\mathcal{A}^{\text{disk}}(\mathcal{V})$ has a nontrivial dependence on λ_{BCFT} . We choose

$$\mathcal{V} = -\frac{2i}{\alpha'} c\tilde{c}\partial X\bar{\partial}X. \quad (3.7)$$

The normalization of \mathcal{V} is the same as that in [29]. The dependence of $\mathcal{A}^{\text{disk}}(\mathcal{V})$ on λ_{BCFT} can be easily determined using the boundary state [30], as studied, for example, in [31]. We have

$$\mathcal{A}^{\text{disk}}(\mathcal{V}) \propto \cos(2\pi\lambda_{\text{BCFT}}). \quad (3.8)$$

It is a periodic function of λ_{BCFT} , and the Dirichlet boundary condition corresponds to the point $\lambda_{\text{BCFT}} = 1/2$. The overall normalization of $\mathcal{A}^{\text{disk}}(\mathcal{V})$ can be determined by evaluating the one-point function of \mathcal{V} on a disk with the Neumann boundary condition, which corresponds to $\lambda_{\text{BCFT}} = 0$. Our normalization of correlation functions on the upper half-plane is

$$\langle c(z_1) c(z_2) c(z_3) \rangle_{\text{UHP}} = (z_1 - z_2)(z_1 - z_3)(z_2 - z_3). \quad (3.9)$$

Here and in what follows we divide correlation functions by the spacetime volume factor. The one-point function of \mathcal{V} on the upper half-plane with the Neumann boundary condition is given by

$$-\frac{1}{\pi} \frac{1}{1+t^2} \left(-\frac{2i}{\alpha'} \right) \langle c\bar{c}\partial X \bar{\partial} X(i) c(t) \rangle_{\text{UHP}} = -\frac{1}{2\pi}. \quad (3.10)$$

This fixes the overall normalization of $\mathcal{A}^{\text{disk}}(\mathcal{V})$ to give

$$\mathcal{A}^{\text{disk}}(\mathcal{V}) = -\frac{1}{2\pi} \cos(2\pi\lambda_{\text{BCFT}}). \quad (3.11)$$

Using the relation (3.6) we have

$$W(\Psi, \mathcal{V}) = -\frac{1}{2\pi} \left[\cos(2\pi\lambda_{\text{BCFT}}) - 1 \right]. \quad (3.12)$$

It is convenient to introduce

$$W_{XX} \equiv 1 - 2\pi W(\Psi, \mathcal{V}) \quad (3.13)$$

for \mathcal{V} given by (3.7). Then we have

$$W_{XX} = \cos(2\pi\lambda_{\text{BCFT}}). \quad (3.14)$$

As we mentioned before, the left-hand side is a function of λ_{SFT} labeling the solutions so that we can derive a map between λ_{SFT} and λ_{BCFT} from this relation. In particular, the value of the gauge-invariant observable for the solution corresponding to the Dirichlet boundary condition $\lambda_{\text{BCFT}} = 1/2$ is given by $W_{XX} = -1$.

4 Evaluation of the gauge-invariant observables

In this section we illustrate our computation of the gauge-invariant observables for the solutions corresponding to the cosine deformations reviewed in section 2. The solutions in Siegel gauge were constructed by Sen and Zwiebach in [22] up to level 4. We expand the string field in level ℓ as follows:

$$|\Psi\rangle = \sum_{\ell=0}^{\infty} |\Psi^{(\ell)}\rangle. \quad (4.1)$$

The expressions up to level 4 in the notation used in section 3 of [22] are given by

$$\begin{aligned}
|\Psi^{(0)}\rangle &= t_0 c_1 |0\rangle, \\
|\Psi^{(1)}\rangle &= t_1 : \cos \frac{X(0)}{\sqrt{\alpha'}} : c_1 |0\rangle, \\
|\Psi^{(2)}\rangle &= (u_0 c_{-1} b_{-1} + v_0 L_{-2}^X + w_0 L'_{-2}) c_1 |0\rangle, \\
|\Psi^{(3)}\rangle &= (u_1 c_{-1} b_{-1} + v_1 L_{-2}^X + w_1 L'_{-2} + z_1 L_{-1}^X L'_{-1}) |\varphi_t\rangle \quad \text{with} \quad |\varphi_t\rangle = : \cos \frac{X(0)}{\sqrt{\alpha'}} : c_1 |0\rangle, \\
|\Psi^{(4)}\rangle &= \tilde{g} |p_4\rangle + t_2 |\chi\rangle + \left[a L_{-4}^X + \bar{a} L'_{-4} + b L_{-2}^X L_{-2}^X + \bar{b} L'_{-2} L'_{-2} + \hat{b} L'_{-2} L_{-2}^X \right. \\
&\quad \left. + c c_{-3} b_{-1} + d b_{-3} c_{-1} + e b_{-2} c_{-2} + (f L_{-2}^X + \bar{f} L'_{-2}) c_{-1} b_{-1} \right] c_1 |0\rangle,
\end{aligned} \tag{4.2}$$

where L_n^X are the Virasoro generators associated with the field $X(t)$ describing the compactified direction and L'_n are the Virasoro generators associated with the rest of the matter fields. The primary field $|p_4\rangle$ at level 4 is given by

$$|p_4\rangle = \left(\alpha_{-3}^X \alpha_{-1}^X - \frac{3}{4} (\alpha_{-2}^X)^2 - \frac{1}{2} (\alpha_{-1}^X)^4 \right) c_1 |0\rangle, \tag{4.3}$$

and $|\chi\rangle$ is

$$|\chi\rangle = : \cos \frac{2X(0)}{\sqrt{\alpha'}} : |0\rangle. \tag{4.4}$$

The gauge-invariant observable $W(\phi, \mathcal{V})$ can be expressed as a BPZ inner product of ϕ with an open string state. For \mathcal{V} given by (3.7), the gauge-invariant observable is

$$W(\phi, \mathcal{V}) = \langle \Phi_{XX}, \phi \rangle, \tag{4.5}$$

where the open string state Φ_{XX} has been constructed in [29] and is given by

$$|\Phi_{XX}\rangle = \left(\frac{1}{4} - 4 \sum_{n,m=1}^{\infty} i^{m-n} m n \alpha_{-m}^X \alpha_{-n}^X \right) e^E c_0 c_1 |0\rangle \tag{4.6}$$

with

$$E = -\frac{1}{2} \sum_{n=1}^{\infty} \frac{(-1)^n}{n} \alpha_{-n} \cdot \alpha_{-n} + \sum_{n=1}^{\infty} (-1)^n c_{-n} b_{-n}. \tag{4.7}$$

We denote the gauge-invariant observable $W(\Psi, \mathcal{V})$ truncated to level ℓ by $W^{(\ell)}(\Psi, \mathcal{V})$. The quantity $W^{(4)}(\Psi, \mathcal{V})$ is given by

$$\begin{aligned}
W^{(4)}(\Psi, \mathcal{V}) &= \sum_{\ell=0}^4 \langle \Phi_{XX}, \Psi^{(\ell)} \rangle \\
&= \frac{1}{4} t_0 + \frac{1}{4} u_0 - \frac{31}{8} v_0 + \frac{25}{8} w_0 + \frac{31}{4} a - \frac{25}{4} \bar{a} + \frac{963}{16} b + \frac{675}{16} \bar{b} - \frac{775}{16} \hat{b} \\
&\quad + \frac{1}{4} e - \frac{31}{8} f + \frac{25}{8} \bar{f} + 192 \tilde{g}.
\end{aligned} \tag{4.8}$$

Note that there are no contributions from $\Psi^{(1)}$ and $\Psi^{(3)}$ because of momentum conservation.

In the numerical solution constructed by Sen and Zwiebach in [22], the component fields t_0, t_1, u_0, \dots are given as functions of t_1 . We therefore obtain $W^{(4)}(\Psi, \mathcal{V})$ for the solution as a function of t_1 , which we are using as the label λ_{SFT} . This is how we compute the gauge-invariant observable as a function of λ_{SFT} in level truncation. We then compare the result with the expression (3.12) of the gauge-invariant observable as a function of λ_{BCFT} to find a relation between λ_{SFT} and λ_{BCFT} numerically.

5 Numerical evaluation to level 12

The method illustrated in the preceding section at level 4 can be extended to higher levels. We had generated all required vertices using the conservation laws of [32] and then solved the equations of motion by Newton's iterative method.³ With the help of a computer cluster we were able to perform all our computations to level (12, 36).

To avoid possible confusion between the marginal and vacuum branches, but also out of curiosity, we studied numerically both branches for various values of λ , up to the critical level-dependent λ_{crit} , where both branches meet. The value of λ_{crit} at level 1 is given by the simple analytic formula (2.5). At higher levels we employed the interval bisection method and studied whether Newton's method converges for given λ . The results are given in table 1. Interestingly,

L	λ_{crit}	L	λ_{crit}
1	0.419026	7	0.469239
2	0.454866	8	0.468645
3	0.467900	9	0.468623
4	0.468614	10	0.468160
5	0.469761	11	0.468109
6	0.469100	12	0.467748

Table 1: Results for λ_{crit} at levels $L = 1, \dots, 12$. The values are rounded down to six digits, so that the solution still exists for these values. It can be found within about 5 iterations if we use as the starting point for Newton's method the highest λ solution found in the previous steps at the same level. Increasing the last digit by one, Newton's method would not anymore converge within 50 iterations at lower levels and at least 10 iterations at level 12.

³ Newton's method requires a choice of an initial approximate solution, which is then iteratively improved to any desired accuracy. We define it as $\frac{\|\Psi^{(i)} - \psi^{(i-1)}\|}{\|\psi^{(i)}\|}$ and stop the iteration when we reach 10^{-8} . The norm is defined, as usual, by a square root of the sum of coefficients squared in the basis formed by α oscillators of the compact direction, bc oscillators of the ghost sector, and the Virasoro generators in the rest of the matter sector. As the starting point we either used results for the solution with the same λ found at lower level or, sometimes more efficiently, used a different solution with a neighboring value of λ at the same level.

the critical value grows at low levels and is largest at level 5, and after one oscillation it monotonically decreases. Simple linear extrapolation in $1/L$ to the infinite level gives the critical value of about 0.466. Values of the energy and the gauge-invariant observables at λ_{crit} for each given level $L = 1, \dots, 12$ are presented in table 3 of appendix A.

We have constructed the marginal and vacuum branches for about 15 different values of λ . Figure 2, presented in section 2, shows the energy density of the marginal and vacuum branches meeting at λ_{crit} . The quantity W_{XX} defined in (3.13) on the marginal branch for various levels is plotted in the left graph of figure 3. Its dependence on the level is rather erratic, so we tried to apply Padé-Borel resummation of contributions of different levels for each solution. The right graph of figure 3 shows the resulting improved values of W_{XX} , together with a simple extrapolation to the infinite level. More data are presented in appendix A.

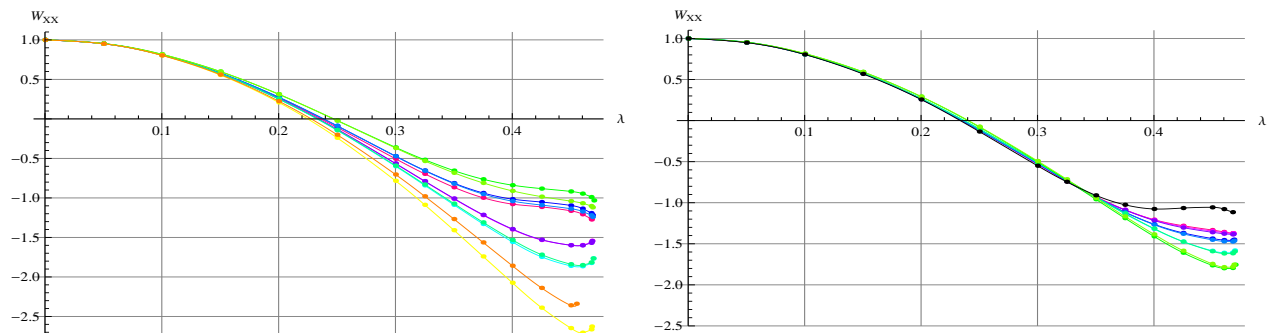


Figure 3: The values of W_{XX} at levels $L = 2, \dots, 12$ (left) and their Padé-Borel improvements at levels $L = 4, \dots, 12$, together with a fit to the infinite level in black (right).

One may notice that starting at level 3 the results at odd levels are close to the values found at the previous even level. The reason is most likely that at even levels new fields with zero momentum appear, and they seem to have larger influence than the fields with nonzero momentum. The similarity of odd and even levels is even greater for W_{XX} because it receives contributions only from fields at even levels, meaning that any change at odd levels can arise only from the change of the solution and not from adding new fields.

Table 2 summarizes linear extrapolations in $1/L$ of various quantities of interest to the infinite level together with the estimated statistical error. We estimate the error by considering extrapolations using different numbers of data points and computing the sample standard deviation for such results. For W_{XX} we use the Padé-Borel resummed version. We also computed W_{00} defined by

$$W_{00} = 1 + 2\pi W(\Psi, \mathcal{V}) \quad (5.1)$$

with

$$\mathcal{V} = -\frac{2i}{\alpha'} c\tilde{c}\partial X^0\bar{\partial}X^0. \quad (5.2)$$

λ	E_{tot}	$\sigma_{E_{tot}}$	E_{kin}	$\sigma_{E_{kin}}$	W_{00}	$\sigma_{W_{00}}$	W_{XX}	$\sigma_{W_{XX}}$
0.05	1.	6.3×10^{-7}	1.	2.1×10^{-7}	1.	0.00007	0.9493	0.0018
0.1	1.	0.00001	1.	3.4×10^{-6}	1.	0.00028	0.8051	0.0025
0.15	1.	0.000051	1.	0.000018	1.0001	0.00066	0.5686	0.0046
0.2	1.	0.00016	1.	0.000057	1.	0.0012	0.2572	0.014
0.25	0.9999	0.0004	1.	0.00014	0.9996	0.002	-0.1338	0.012
0.3	0.9999	0.00083	0.9997	0.00026	0.9978	0.0029	-0.5499	0.0022
0.325	1.	0.0011	0.999	0.00033	0.9954	0.0034	-0.7449	0.01
0.35	1.0004	0.0015	0.9972	0.00041	0.9905	0.0039	-0.9096	0.013
0.375	1.0016	0.0019	0.992	0.00052	0.9798	0.0043	-1.0251	0.027
0.4	1.0049	0.0023	0.9781	0.00035	0.9565	0.0046	-1.076	0.044
0.425	1.013	0.0028	0.9433	0.0013	0.9075	0.005	-1.0649	0.059
0.45	1.0321	0.0035	0.8668	0.0046	0.8116	0.0064	-1.0562	0.076
0.46	1.0451	0.0037	0.8112	0.0067	0.7453	0.0077	-1.0778	0.085
0.4675	1.0585	0.0039	0.7124	0.019	0.6326	0.02	-1.1149	0.092

Table 2: Extrapolation to the infinite level and its possible statistical error for the four basic quantities computed at several values of λ on the marginal branch. Up to about $\lambda = 0.325$ the first three observables are within the 3σ tolerance away from the expected value of 1.

Up to approximately $\lambda = 0.325$ the extrapolated values of the energy density E_{tot} computed from the full action, the energy density E_{kin} computed from the kinetic term, and W_{00} are consistent with the expected value 1. Apparently, for higher values of λ our method underestimates the error of the extrapolated values.

The results for W_{XX} together with its estimated error are presented in figure 4. The one-parameter fit of the form $\cos(2\pi(\lambda + a\lambda^3))$ is also shown, where the constant a has been fitted so that the extrapolation to the infinite level coincides with the boundary CFT result at lower values of λ . The best fit value for a is about 0.99 at level 4 and grows at higher levels. For the extrapolation to the infinite level we find $a \approx 1.48$. It would be interesting to calculate this value analytically. The results of W_{XX} qualitatively agree with the analysis by Sen [23] using the energy-momentum tensor and are consistent with the picture that the finite range of the branch covers one fundamental domain of the periodic moduli space. While our results do not provide sufficient evidence that the branch covers *exactly* one fundamental domain, we can safely exclude the possibility that the branch covers the fundamental domain many times. We can also exclude the opposite possibility that the branch covers, say, less than 75% of the fundamental domain. If the branch indeed covers exactly one fundamental domain, it would be interesting to understand why it is the case.

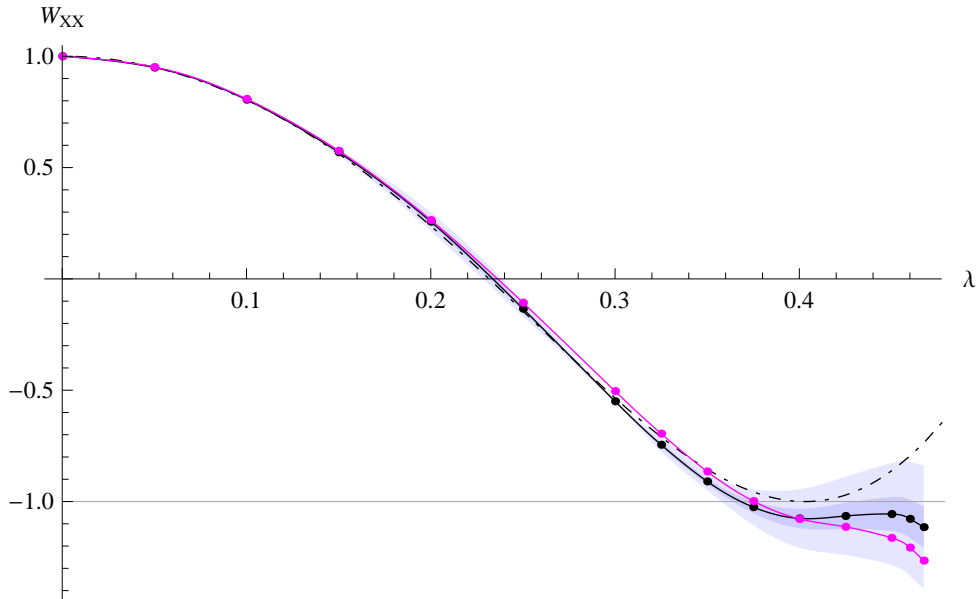


Figure 4: Extrapolation to the infinite level of the Padé-Borel resummed version of W_{XX} . The black solid line is the infinite-level fit itself, while the shaded regions around it indicate σ and 3σ uncertainty ranges in the extrapolation. The magenta line shows the (unimproved) data at level 12 for comparison. The black dot-dashed line is the one-parameter fit of the form $\cos(2\pi(\lambda + a\lambda^3))$.

6 Discussion

In this paper we presented a method of constructing a map between the deformation parameter λ_{BCFT} of boundary CFT and the parameter λ_{SFT} labeling solutions of open string field theory for marginal deformations. While we applied our method to the specific problem of covering moduli for solutions in Siegel gauge, the basic idea is universal and we can use it for other problems. For example, a similar problem for the system of separated D-branes has recently been discussed in [33, 34] and it would be interesting to compute the gauge-invariant observables in the system.

If we construct the boundary state from numerical solutions following the proposal in [35], we will be able to obtain more information on the boundary CFT. However, construction of the boundary state for numerical solutions seems to be challenging. In particular, the closed string state proposed in [35] is conjectured to reproduce the boundary state up to a BRST-exact term, and such a BRST-exact term would obscure the boundary state especially for approximate solutions constructed numerically.⁴

Our results are qualitatively consistent with the analysis by Sen [23] using the energy-

⁴ After this paper was submitted to arXiv, another approach to the construction of the boundary state was proposed in [36], which is more suitable for the application to numerical solutions.

momentum tensor. This is not unexpected because both methods are based on coupling to an infinitesimal closed string field. However, the closed string is described by an unintegrated vertex operator in the gauge-invariant observables and also in the boundary state construction in [35], while the infinitesimal change in the closed string background is related more closely to an integrated vertex operator. It would be an interesting problem to convert the unintegrated vertex operator to the integrated vertex operator in the framework of the gauge-invariant observables and the boundary state construction [35].

Acknowledgments

We would like to thank Ted Erler, Mitsuhiro Kato, Michael Kiermaier, Carlo Maccaferri and Barton Zwiebach for helpful discussions and to Masaki Murata for careful reading of the manuscript. The access to computing and storage facilities owned by parties and projects contributing to the Czech National Grid Infrastructure MetaCentrum, provided under the programme “Projects of Large Infrastructure for Research, Development, and Innovations” (LM2010005), and to CERIT-SC computing facilities provided under the programme Center CERIT Scientific Cloud, part of the Operational Program Research and Development for Innovations, reg. no. CZ. 1.05/3.2.00/08.0144 is highly appreciated. The work of Y.O. was supported in part by Grant-in-Aid for Scientific Research (B) No. 20340048 and Grant-in-Aid for Scientific Research (C) No. 24540254 from the Japan Society for the Promotion of Science (JSPS). The work of M.S. was supported by the EURYI grant GACR EYI/07/E010 from EUROHORC and ESF. The work of Y.O. and M.S. was also supported in part by the MŠMT contract No. LH11106 and by JSPS and the Academy of Sciences of the Czech Republic (ASCR) under the Research Cooperative Program between Japan and the Czech Republic.

A Tables of numerical results

In the following figures E_{tot} denotes the energy density computed from the full action and E_{kin} denotes the energy density computed from the kinetic term.

L/λ	0	0.05	0.1	0.15	0.2	0.25	0.3	0.325
1	1	1.00003	1.00042	1.00216	1.00694	1.01739	1.03737	1.05266
2	1	1.00001	1.0001	1.00056	1.0019	1.00515	1.01209	1.01789
3	1	1.00001	1.0001	1.00054	1.00179	1.00473	1.01084	1.01585
4	1	1.	1.00005	1.00027	1.00095	1.00264	1.00644	1.00976
5	1	1.	1.00005	1.00027	1.00091	1.00249	1.00598	1.009
6	1	1.	1.00003	1.00018	1.00062	1.00175	1.00436	1.00672
7	1	1.	1.00003	1.00017	1.00061	1.00168	1.00413	1.00634
8	1	1.	1.00002	1.00013	1.00046	1.00131	1.0033	1.00515
9	1	1.	1.00002	1.00013	1.00045	1.00127	1.00317	1.00492
10	1	1.	1.00002	1.0001	1.00037	1.00104	1.00266	1.00418
11	1	1.	1.00002	1.0001	1.00036	1.00102	1.00258	1.00403
12	1	1.	1.00002	1.00009	1.00031	1.00087	1.00223	1.00353

L/λ	0.35	0.375	0.4	0.425	0.45	0.46	0.4675
1	1.07282	1.09934	1.13463	—	—	—	—
2	1.02604	1.03744	1.05342	1.07621	1.11061	—	—
3	1.02282	1.03249	1.04595	1.06492	1.09248	1.10738	1.12122
4	1.01461	1.02171	1.03215	1.04775	1.07183	1.08537	1.09816
5	1.01342	1.01992	1.02957	1.04421	1.06719	1.08023	1.09249
6	1.01029	1.01572	1.02413	1.03747	1.05938	1.07219	1.08449
7	1.00967	1.01478	1.02277	1.03565	1.05721	1.06995	1.08221
8	1.008	1.01249	1.01977	1.03192	1.05302	1.06575	1.07818
9	1.00763	1.01191	1.01891	1.0308	1.05177	1.06453	1.07701
10	1.00658	1.01045	1.01696	1.02837	1.04912	1.06193	1.0746
11	1.00632	1.01005	1.01636	1.02759	1.04831	1.06117	1.07391
12	1.0056	1.00902	1.01497	1.02587	1.04647	1.0594	1.07233

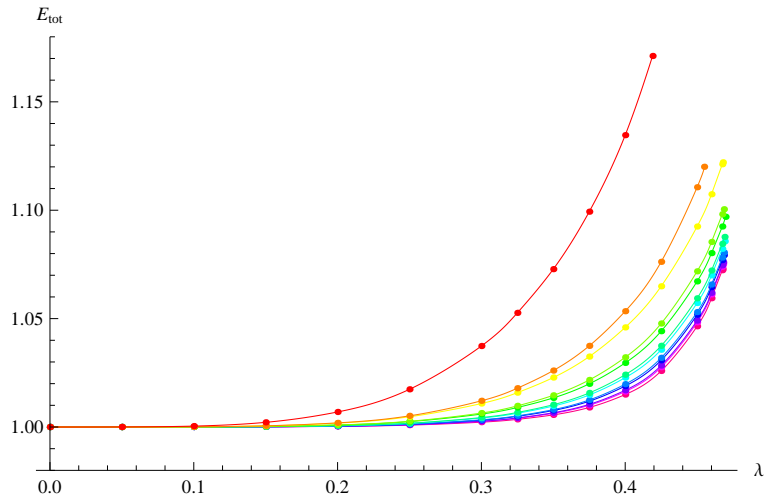


Figure 5: E_{tot} for the marginal branch at levels $L = 1, \dots, 12$. For the color legend, see figure 15.

L/λ	0	0.05	0.1	0.15	0.2	0.25	0.3	0.325
1	1	0.999991	0.999857	0.999248	0.997483	0.993325	0.984406	0.976723
2	1	0.999998	0.999962	0.999776	0.999134	0.997311	0.992653	0.988209
3	1	0.999998	0.999964	0.999796	0.999243	0.997733	0.993941	0.990326
4	1	0.999999	0.999981	0.999887	0.999541	0.998487	0.995519	0.99246
5	1	0.999999	0.999982	0.999893	0.999581	0.998645	0.996008	0.993251
6	1	0.999999	0.999988	0.999925	0.999692	0.998949	0.996713	0.994255
7	1	0.999999	0.999988	0.999928	0.999711	0.999028	0.996974	0.994692
8	1	1.	0.999991	0.999944	0.999769	0.999194	0.997387	0.99531
9	1	1.	0.999991	0.999946	0.999779	0.999241	0.99755	0.99559
10	1	1.	0.999993	0.999956	0.999815	0.999346	0.997825	0.996017
11	1	1.	0.999993	0.999957	0.999821	0.999376	0.997936	0.996215
12	1	1.	0.999994	0.999963	0.999845	0.999449	0.998134	0.99653

L/λ	0.35	0.375	0.4	0.425	0.45	0.46	0.4675
1	0.965317	0.947508	0.915633	—	—	—	—
2	0.981281	0.970361	0.952595	0.921238	0.844668	—	—
3	0.984677	0.975766	0.961401	0.937109	0.890234	0.853796	0.787548
4	0.987406	0.978993	0.964745	0.939657	0.890215	0.852261	0.792049
5	0.988608	0.980684	0.966887	0.941989	0.892573	0.855588	0.80361
6	0.989951	0.982294	0.968387	0.942343	0.889422	0.849383	0.790421
7	0.990629	0.983238	0.969448	0.942981	0.888695	0.847973	0.789345
8	0.9915	0.98433	0.970452	0.942955	0.885679	0.8425	0.776961
9	0.991952	0.984971	0.971128	0.943099	0.884412	0.84051	0.774259
10	0.992581	0.985794	0.971888	0.942936	0.881779	0.835993	0.762596
11	0.99291	0.986275	0.972377	0.942887	0.88049	0.834132	0.759646
12	0.993391	0.98693	0.972985	0.942661	0.878228	0.830423	0.747139

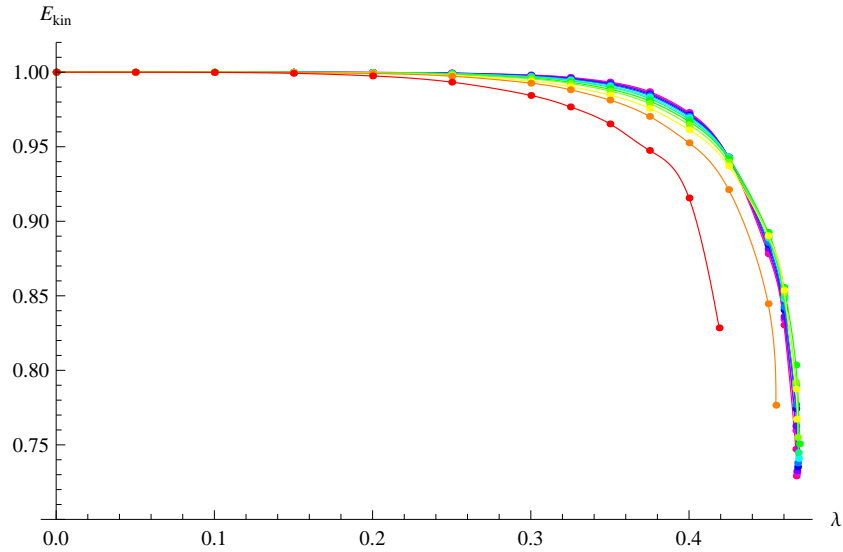


Figure 6: E_{kin} for the marginal branch at levels $L = 1, \dots, 12$.

L/λ	0	0.05	0.1	0.15	0.2	0.25	0.3	0.325
1	1	0.99744	0.989648	0.976257	0.956556	0.929248	0.891855	0.867871
2	1	0.999327	0.99716	0.993028	0.986042	0.974681	0.956329	0.94316
3	1	0.999329	0.997202	0.993246	0.986732	0.976369	0.95985	0.94805
4	1	0.99966	0.998549	0.996363	0.99248	0.98572	0.973796	0.964585
5	1	0.999661	0.998565	0.996445	0.992747	0.986396	0.975226	0.966539
6	1	0.999773	0.999025	0.997524	0.994784	0.989816	0.980526	0.972937
7	1	0.999774	0.999033	0.997567	0.994926	0.990191	0.981362	0.974112
8	1	0.999835	0.999286	0.998173	0.9961	0.992236	0.984701	0.978279
9	1	0.999835	0.999291	0.998197	0.996186	0.99247	0.985248	0.97907
10	1	0.999867	0.999423	0.998518	0.996816	0.993596	0.987151	0.981498
11	1	0.999867	0.999426	0.998534	0.996874	0.993756	0.987539	0.982073
12	1	0.999891	0.999528	0.998781	0.997362	0.994636	0.989057	0.98404

L/λ	0.35	0.375	0.4	0.425	0.45	0.46	0.4675
1	0.838716	0.801585	0.748454	—	—	—	—
2	0.926096	0.90354	0.872612	0.826695	0.735129	—	—
3	0.932795	0.912723	0.885576	0.846949	0.784627	0.74208	0.672205
4	0.951971	0.934369	0.909122	0.871148	0.807038	0.762761	0.697553
5	0.954519	0.937497	0.91265	0.874683	0.81039	0.767018	0.709998
6	0.962023	0.945903	0.921317	0.882148	0.813582	0.766378	0.701007
7	0.963589	0.947821	0.923321	0.883583	0.813501	0.765561	0.700451
8	0.96866	0.953717	0.929562	0.888897	0.815361	0.764379	0.691122
9	0.969747	0.955078	0.930943	0.889626	0.814543	0.762767	0.688646
10	0.97277	0.958646	0.934636	0.89228	0.814131	0.759898	0.677343
11	0.973583	0.959691	0.935684	0.892684	0.813174	0.758292	0.674445
12	0.976086	0.96273	0.938921	0.895071	0.813104	0.756321	0.662292

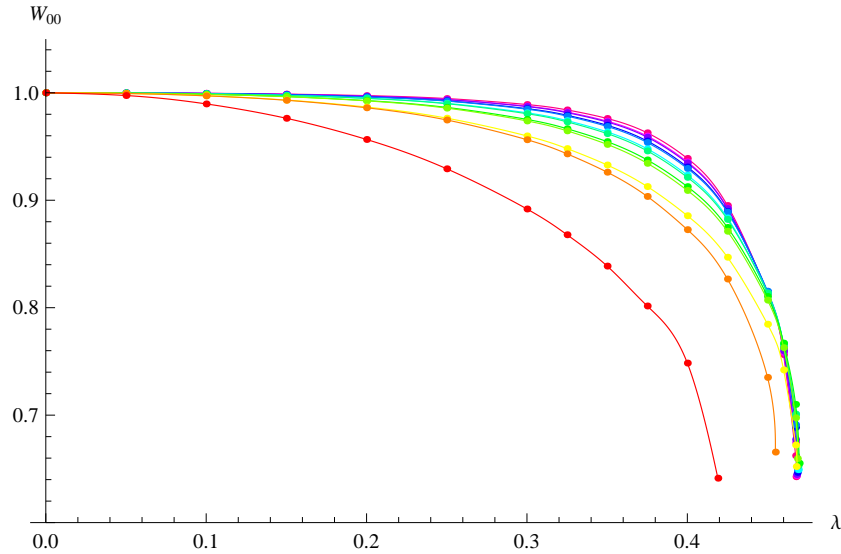


Figure 7: W_0 for the marginal branch at levels $L = 1, \dots, 12$.

L/λ	0	0.05	0.1	0.15	0.2	0.25	0.3	0.325
1	1	0.99744	0.989648	0.976257	0.956556	0.929248	0.891855	0.867871
2	1	0.951001	0.804391	0.561486	0.225054	-0.199654	-0.703015	-0.979158
3	1	0.950938	0.803384	0.55637	0.208866	-0.238966	-0.782912	-1.08704
4	1	0.953882	0.817906	0.599563	0.312592	-0.020983	-0.368017	-0.532577
5	1	0.953879	0.817865	0.599431	0.312586	-0.019437	-0.35992	-0.516995
6	1	0.9517	0.808058	0.572963	0.253324	-0.140082	-0.590749	-0.82979
7	1	0.951696	0.807988	0.572595	0.252092	-0.143343	-0.598223	-0.840638
8	1	0.952127	0.810397	0.580849	0.274993	-0.087298	-0.471833	-0.655231
9	1	0.952126	0.810381	0.580781	0.274838	-0.087384	-0.470778	-0.652329
10	1	0.951473	0.807389	0.572431	0.255112	-0.130855	-0.563695	-0.787236
11	1	0.951472	0.807373	0.572346	0.254826	-0.13161	-0.565422	-0.789735
12	1	0.951627	0.808281	0.575623	0.264426	-0.106573	-0.504102	-0.694964

L/λ	0.35	0.375	0.4	0.425	0.45	0.46	0.4675
1	0.838716	0.801585	0.748454	-	-	-	-
2	-1.26737	-1.56275	-1.85779	-2.13867	-2.35874	-	-
3	-1.40816	-1.74019	-2.07303	-2.38872	-2.64695	-2.70528	-2.66319
4	-0.682196	-0.810004	-0.910679	-0.98362	-1.04015	-1.06733	-1.10254
5	-0.654344	-0.76347	-0.838485	-0.88199	-0.91762	-0.94553	-0.98925
6	-1.07165	-1.30896	-1.53045	-1.71789	-1.83833	-1.84958	-1.81515
7	-1.08692	-1.32954	-1.55612	-1.74542	-1.85932	-1.86422	-1.823
8	-0.819198	-0.951134	-1.04046	-1.09027	-1.13631	-1.17153	-1.2199
9	-0.812499	-0.937299	-1.01516	-1.05217	-1.095	-1.13498	-1.19199
10	-1.00706	-1.21363	-1.39341	-1.52837	-1.59857	-1.60014	-1.5681
11	-1.01053	-1.21815	-1.39839	-1.53177	-1.59746	-1.59668	-1.56202
12	-0.865035	-0.997802	-1.07794	-1.11365	-1.16324	-1.20662	-1.26519

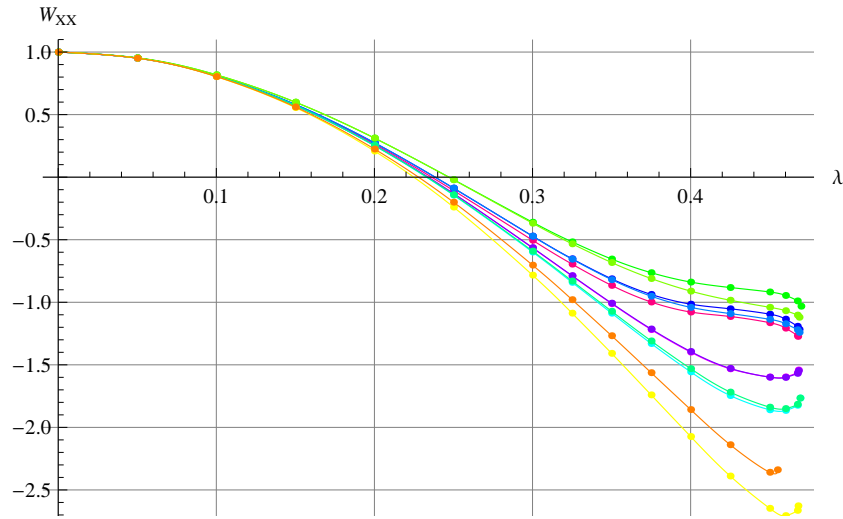


Figure 8: W_{XX} for the marginal branch at levels $L = 2, \dots, 12$.

L/λ	0	0.05	0.1	0.15	0.2	0.25	0.3	0.325
4	1	0.953629	0.816342	0.593424	0.29318	-0.073308	-0.491522	-0.713913
5	1	0.953623	0.81625	0.592937	0.291551	-0.07754	-0.50075	-0.726754
6	1	0.954787	0.807347	0.577341	0.26935	-0.100336	-0.509693	-0.720384
7	1	0.95479	0.807286	0.57709	0.268623	-0.101967	-0.512727	-0.72423
8	1	0.951803	0.808898	0.576478	0.263759	-0.115659	-0.519682	-0.731568
9	1	0.951802	0.808879	0.576382	0.263459	-0.116387	-0.521665	-0.733233
10	1	0.95142	0.808035	0.576461	0.261433	-0.114106	-0.526226	-0.736616
11	1	0.951419	0.808023	0.576385	0.26121	-0.114446	-0.527015	-0.738181
12	1	0.951444	0.807564	0.574423	0.264885	-0.117854	-0.529692	-0.734165

L/λ	0.35	0.375	0.4	0.425	0.45	0.46	0.4675
4	-0.940565	-1.16652	-1.38471	-1.58423	-1.74414	-1.78381	-1.78005
5	-0.95765	-1.18798	-1.40947	-1.60904	-1.76267	-1.79768	-1.79456
6	-0.928999	-1.12958	-1.31443	-1.47336	-1.59101	-1.61814	-1.61616
7	-0.93354	-1.1343	-1.31804	-1.47347	-1.58483	-1.60904	-1.60543
8	-0.933027	-1.11522	-1.26675	-1.37868	-1.4516	-1.47037	-1.47305
9	-0.934061	-1.11437	-1.26179	-1.36752	-1.43568	-1.45435	-1.45846
10	-0.931459	-1.08781	-1.21579	-1.30324	-1.35948	-1.37767	-1.38591
11	-0.930263	-1.085	-1.20917	-1.29144	-1.34508	-1.36402	-1.37425
12	-0.923884	-1.08608	-1.20608	-1.28016	-1.33251	-1.35569	-1.3723

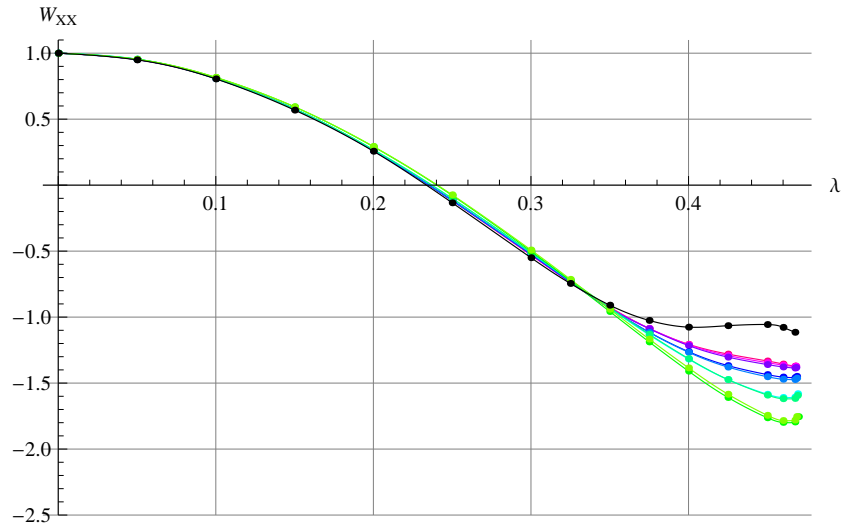


Figure 9: Padé-Borel improvement of W_{XX} for the marginal branch at levels $L = 4, \dots, 12$. The black curve shows the pointwise extrapolation to the infinite level.

L/λ	0	0.05	0.1	0.15	0.2	0.25	0.3	0.325
1	0.315384	0.329979	0.37345	0.444823	0.542391	0.663537	0.804395	0.880485
2	0.0406234	0.0572608	0.106764	0.18788	0.298435	0.435177	0.593475	0.678748
3	0.0406234	0.0561167	0.102266	0.178062	0.28175	0.410703	0.561182	0.642914
4	0.0121782	0.0277856	0.0742714	0.150608	0.255009	0.384804	0.536189	0.61837
5	0.0121782	0.0276126	0.0735889	0.149108	0.252436	0.38098	0.531054	0.612606
6	0.0048229	0.0202735	0.0662973	0.141892	0.245318	0.373974	0.524159	0.60576
7	0.0048229	0.020213	0.0660582	0.141365	0.24441	0.372619	0.52233	0.603702
8	0.0020698	0.0174607	0.0633076	0.138615	0.241657	0.369853	0.519535	0.600883
9	0.0020698	0.0174318	0.0631933	0.138363	0.24122	0.369198	0.518647	0.599882
10	0.0008175	0.0161771	0.0619308	0.137086	0.23992	0.367862	0.517257	0.598456
11	0.0008175	0.0161608	0.061866	0.136942	0.239671	0.367487	0.516748	0.597881
12	0.0001777	0.0155179	0.0612139	0.136273	0.238977	0.366755	0.515962	0.597061

L/λ	0.35	0.375	0.4	0.425	0.45	0.46	0.4675
1	0.95902	1.03852	1.11653	—	—	—	—
2	0.766716	0.856006	0.944791	1.03037	1.10745	—	—
3	0.72786	0.814928	0.902695	0.989157	1.071	1.10095	1.12114
4	0.703742	0.791192	0.879266	0.965916	1.04775	1.07762	1.0978
5	0.697405	0.784373	0.872105	0.958624	1.04067	1.07082	1.09143
6	0.690596	0.777582	0.865298	0.951738	1.03357	1.06352	1.08384
7	0.688329	0.775138	0.86273	0.949121	1.03102	1.06106	1.08148
8	0.685475	0.772236	0.859756	0.946035	1.02772	1.0576	1.07778
9	0.684371	0.771044	0.858503	0.944762	1.02649	1.05641	1.07662
10	0.6829	0.769518	0.856904	0.94306	1.02462	1.05441	1.07443
11	0.682265	0.768832	0.856183	0.942329	1.02391	1.05373	1.07376
12	0.681404	0.767921	0.855208	0.941268	1.02271	1.05243	1.07229

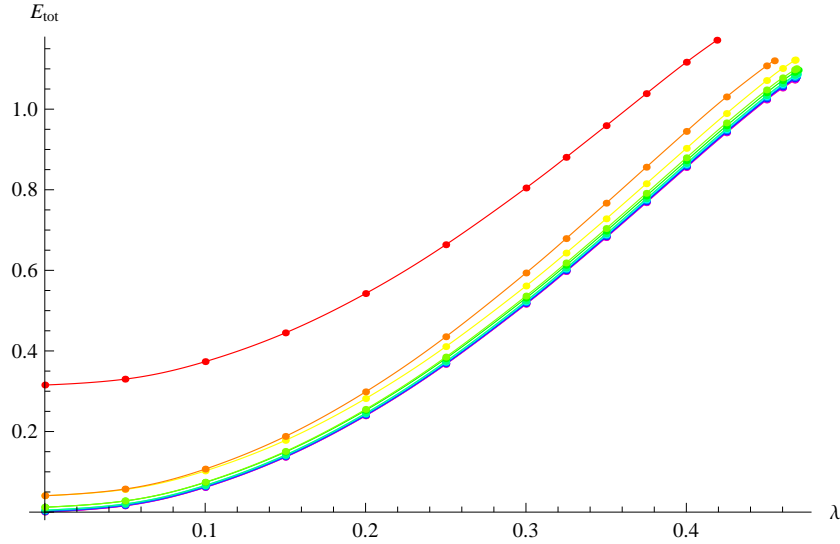


Figure 10: E_{tot} for the vacuum branch at levels $L = 1, \dots, 12$.

L/λ	0	0.05	0.1	0.15	0.2	0.25	0.3	0.325
1	0.315384	0.320266	0.335022	0.36	0.395882	0.443905	0.506437	0.544583
2	0.0406234	0.0461918	0.0630362	0.0915988	0.132712	0.187795	0.259302	0.302519
3	0.0406234	0.0458061	0.0614663	0.087961	0.125963	0.17662	0.241908	0.281081
4	0.0121782	0.0173993	0.0331765	0.0598732	0.0981732	0.149243	0.215096	0.254627
5	0.0121782	0.0173411	0.0329406	0.0593293	0.0971705	0.147593	0.212543	0.25149
6	0.0048229	0.00999118	0.0256074	0.0520254	0.0899106	0.140397	0.20544	0.244454
7	0.0048229	0.00997086	0.0255251	0.0518362	0.0895621	0.139823	0.204548	0.243353
8	0.0020698	0.00721809	0.0227735	0.049087	0.0868182	0.137089	0.201835	0.24066
9	0.0020698	0.0072084	0.0227343	0.0489971	0.0866528	0.136817	0.201409	0.240132
10	0.0008175	0.00595534	0.021479	0.0477386	0.085391	0.135553	0.200149	0.238879
11	0.0008175	0.00594987	0.0214569	0.047688	0.0852981	0.1354	0.199909	0.23858
12	0.0001777	0.00530908	0.0208133	0.0470401	0.084645	0.134742	0.199249	0.237923

L/λ	0.35	0.375	0.4	0.425	0.45	0.46	0.4675
1	0.588887	0.642031	0.711679	—	—	—	—
2	0.351907	0.40904	0.476817	0.561987	0.69613	—	—
3	0.325539	0.376472	0.435932	0.50811	0.605178	0.662188	0.743998
4	0.299516	0.350982	0.411133	0.48427	0.582767	0.640283	0.71504
5	0.295674	0.346272	0.405313	0.476921	0.572739	0.627705	0.692817
6	0.288728	0.339459	0.398721	0.470764	0.567818	0.624362	0.695134
7	0.287373	0.337786	0.396641	0.468137	0.564356	0.620319	0.689695
8	0.28471	0.335177	0.394136	0.465871	0.562898	0.620073	0.695342
9	0.284057	0.334364	0.393115	0.464569	0.561196	0.618168	0.693439
10	0.282817	0.333153	0.391966	0.463577	0.560778	0.618688	0.700398
11	0.282444	0.332686	0.391375	0.462815	0.559781	0.617605	0.699945
12	0.281795	0.332055	0.390786	0.462338	0.559735	0.618308	0.708963

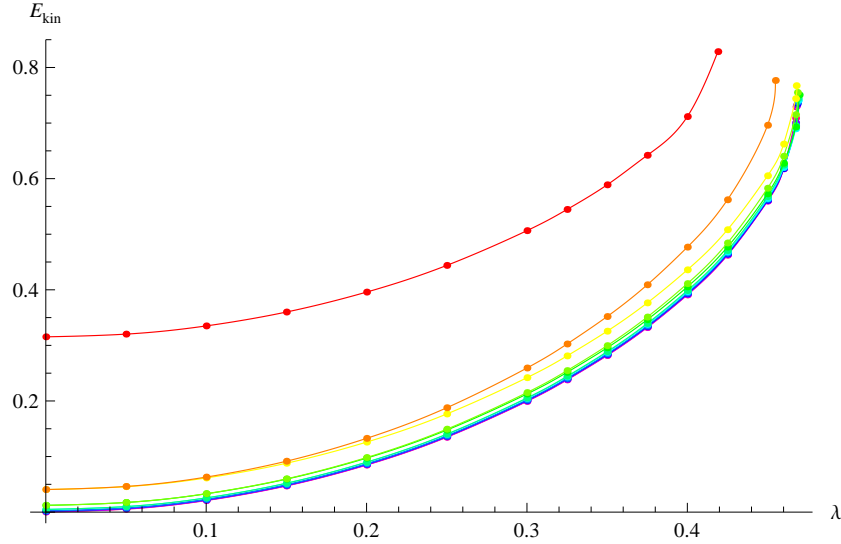


Figure 11: E_{kin} for the vacuum branch at levels $L = 1, \dots, 12$.

L/λ	0	0.05	0.1	0.15	0.2	0.25	0.3	0.325
1	0.283437	0.285997	0.293789	0.30718	0.326882	0.35419	0.391582	0.415566
2	0.110138	0.113727	0.124619	0.143208	0.170241	0.207002	0.25574	0.285807
3	0.110138	0.113299	0.122891	0.139264	0.163072	0.195438	0.238292	0.264667
4	0.0680476	0.0714674	0.0818461	0.0995642	0.125339	0.160392	0.206829	0.235422
5	0.0680476	0.0713873	0.0815236	0.0988297	0.124009	0.158261	0.203649	0.231603
6	0.0489211	0.0523251	0.0626591	0.0803113	0.106014	0.141016	0.187472	0.216127
7	0.0489211	0.0522914	0.0625236	0.0800035	0.105459	0.14013	0.186158	0.214556
8	0.0388252	0.0422404	0.05261	0.0703287	0.0961407	0.131317	0.178048	0.206902
9	0.0388252	0.0422213	0.0525333	0.0701549	0.0958282	0.13082	0.177316	0.206028
10	0.0318852	0.0353054	0.0456915	0.0634425	0.0893108	0.124581	0.171472	0.200444
11	0.0318852	0.0352931	0.0456419	0.0633303	0.0891098	0.124263	0.171004	0.199886
12	0.0274405	0.0308689	0.0412807	0.0590784	0.0850208	0.120403	0.167463	0.196553

L/λ	0.35	0.375	0.4	0.425	0.45	0.46	0.4675
1	0.444721	0.481853	0.534983	—	—	—	—
2	0.320791	0.362181	0.412733	0.47892	0.591238	—	—
3	0.295248	0.33119	0.374481	0.429179	0.507074	0.555604	0.629843
4	0.268586	0.307574	0.35454	0.413848	0.497985	0.549673	0.62015
5	0.264032	0.30216	0.348087	0.406038	0.487846	0.537216	0.598286
6	0.249417	0.288628	0.335981	0.395973	0.481405	0.533842	0.602502
7	0.247551	0.286425	0.333385	0.392901	0.477692	0.529701	0.597151
8	0.240452	0.280018	0.327884	0.388705	0.475913	0.530177	0.605092
9	0.239417	0.278801	0.326456	0.387033	0.473965	0.52814	0.603253
10	0.234153	0.273942	0.322141	0.38353	0.472071	0.527904	0.610834
11	0.233494	0.273169	0.321237	0.382477	0.470869	0.526706	0.610477
12	0.230412	0.270402	0.318887	0.380741	0.470354	0.527499	0.621024

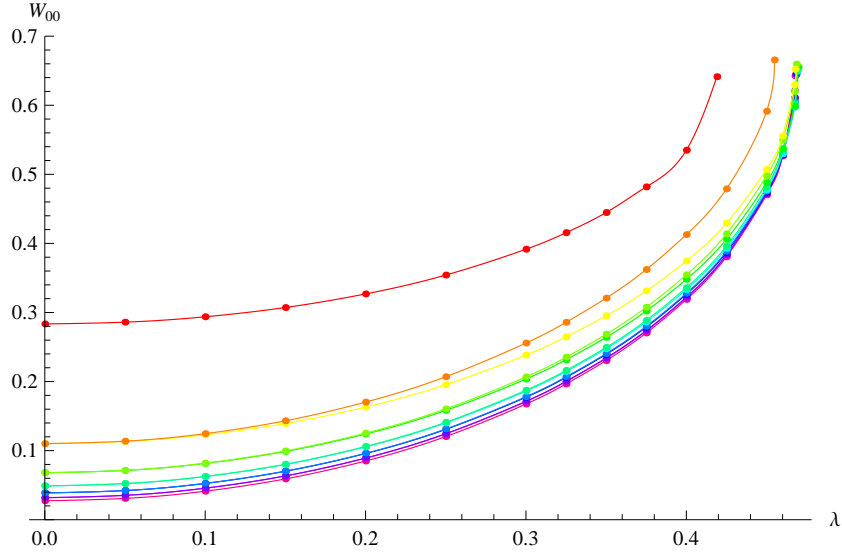


Figure 12: W_{00} for the vacuum branch at levels $L = 1, \dots, 12$.

L/λ	0	0.05	0.1	0.15	0.2	0.25	0.3	0.325
1	0.283437	0.285997	0.293789	0.30718	0.326882	0.35419	0.391582	0.415566
2	0.110138	0.0875615	0.0193784	-0.0958322	-0.260671	-0.479375	-0.758784	-0.92461
3	0.110138	0.0893906	0.0265967	-0.0799804	-0.233546	-0.439388	-0.706161	-0.866689
4	0.0680476	0.0496969	-0.0050390	-0.0951681	-0.218875	-0.373213	-0.553475	-0.651065
5	0.0680476	0.0501372	-0.0033118	-0.0914059	-0.21248	-0.363751	-0.540592	-0.636278
6	0.0489211	0.0313177	-0.021478	-0.109444	-0.232628	-0.391325	-0.586511	-0.69853
7	0.0489211	0.0315214	-0.0206724	-0.107665	-0.229551	-0.386693	-0.580163	-0.691308
8	0.0388252	0.0215946	-0.0299634	-0.115428	-0.234027	-0.384488	-0.564713	-0.664932
9	0.0388252	0.0217196	-0.0294676	-0.114329	-0.23211	-0.381561	-0.560599	-0.66015
10	0.0318852	0.0149249	-0.0358963	-0.120404	-0.238325	-0.389336	-0.573202	-0.677496
11	0.0318852	0.0150087	-0.0355634	-0.119663	-0.23703	-0.387355	-0.570422	-0.674281
12	0.0274405	0.01062	-0.0397397	-0.12332	-0.239541	-0.387463	-0.565568	-0.665187

L/λ	0.35	0.375	0.4	0.425	0.45	0.46	0.4675
1	0.444721	0.481853	0.534983	-	-	-	-
2	-1.11066	-1.32032	-1.55916	-1.83858	-2.20227	-	-
3	-1.04892	-1.25712	-1.49816	-1.78477	-2.14961	-2.3441	-2.57644
4	-0.751803	-0.853628	-0.953435	-1.04596	-1.11977	-1.13655	-1.13214
5	-0.734843	-0.83396	-0.929944	-1.01617	-1.07704	-1.08354	-1.06612
6	-0.82101	-0.955211	-1.10355	-1.27139	-1.47483	-1.58038	-1.69678
7	-0.812938	-0.946358	-1.09407	-1.26161	-1.46574	-1.57244	-1.69065
8	-0.770984	-0.881767	-0.995469	-1.10865	-1.21245	-1.24455	-1.25248
9	-0.765464	-0.875398	-0.988039	-1.09967	-1.20044	-1.22985	-1.23252
10	-0.790205	-0.911714	-1.04293	-1.18621	-1.34996	-1.42987	-1.51928
11	-0.786535	-0.90757	-1.03829	-1.18108	-1.34438	-1.42422	-1.51448
12	-0.771212	-0.882866	-0.998863	-1.1167	-1.22961	-1.26769	-1.27831

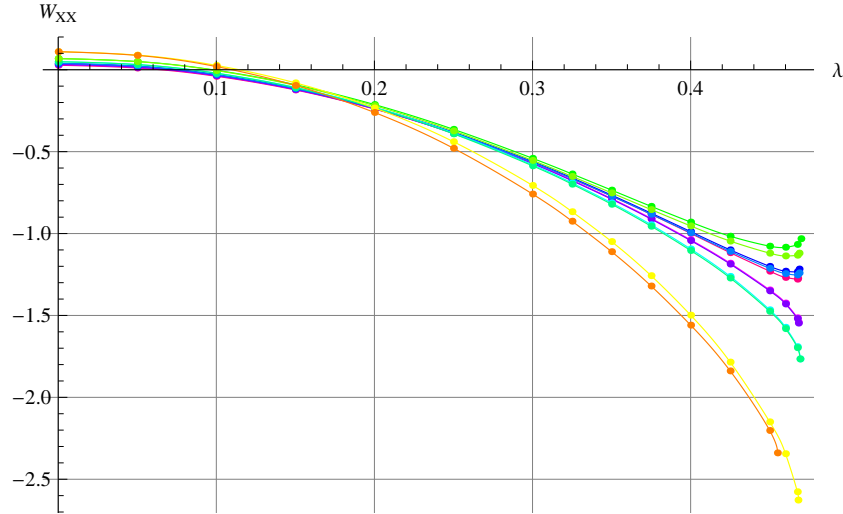


Figure 13: W_{XX} for the vacuum branch at levels $L = 2, \dots, 12$.

L/λ	0	0.05	0.1	0.15	0.2	0.25	0.3	0.325
4	0.0531112	0.0440065	-0.00531479	-0.0958717	-0.223919	-0.388704	-0.590782	-0.706525
5	0.0531112	0.0445574	-0.0035379	-0.0922339	-0.217909	-0.379966	-0.579115	-0.69336
6	0.0390372	0.0220318	-0.0257739	-0.109098	-0.230925	-0.388482	-0.580837	-0.689993
7	0.0390372	0.0222627	-0.0248376	-0.10725	-0.227899	-0.384041	-0.574815	-0.683133
8	0.0309852	0.0160397	-0.034642	-0.118676	-0.234626	-0.392628	-0.574418	-0.672585
9	0.0309852	0.0161757	-0.034102	-0.117464	-0.232628	-0.390156	-0.570038	-0.667684
10	0.0286352	0.0120373	-0.0381778	-0.120848	-0.234825	-0.388183	-0.570068	-0.671444
11	0.0286352	0.0121251	-0.0378259	-0.120048	-0.233877	-0.386267	-0.567252	-0.668102
12	0.0269078	0.00947608	-0.0405434	-0.123708	-0.239038	-0.388482	-0.566975	-0.66749

L/λ	0.35	0.375	0.4	0.425	0.45	0.46	0.4675
4	-0.83294	-0.971294	-1.12392	-1.29564	-1.50001	-1.60228	-1.71059
5	-0.818275	-0.955145	-1.10633	-1.27674	-1.48004	-1.5817	-1.68443
6	-0.80794	-0.935052	-1.07225	-1.22189	-1.39179	-1.47265	-1.5529
7	-0.800211	-0.926413	-1.06263	-1.21114	-1.37956	-1.4596	-1.53858
8	-0.776614	-0.889276	-1.01512	-1.1567	-1.3118	-1.37959	-1.44152
9	-0.771045	-0.882701	-1.00728	-1.14783	-1.302	-1.36894	-1.42939
10	-0.777659	-0.889965	-1.01008	-1.13751	-1.27054	-1.32578	-1.37297
11	-0.773676	-0.885449	-1.00499	-1.13172	-1.26362	-1.31793	-1.36347
12	-0.775368	-0.895805	-1.00836	-1.136	-1.26819	-1.32277	-1.36773

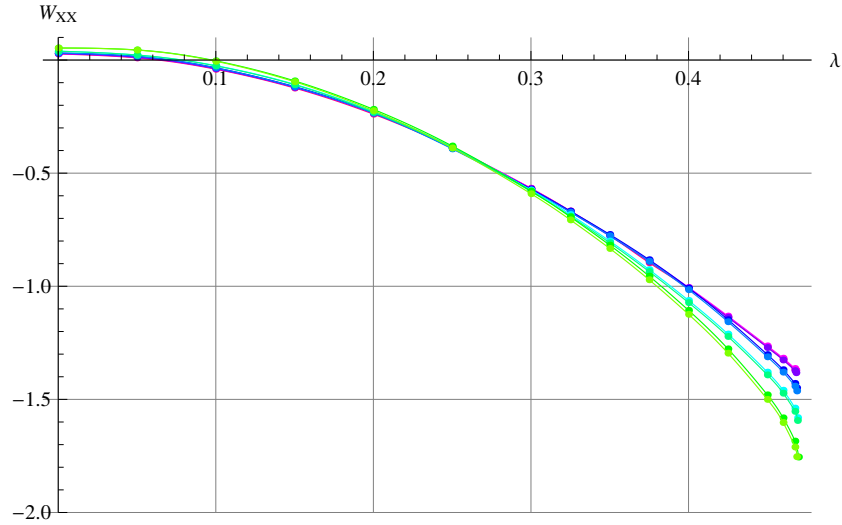


Figure 14: Padé-Borel improvement of W_{XX} for the vacuum branch at levels $L = 4, \dots, 12$.

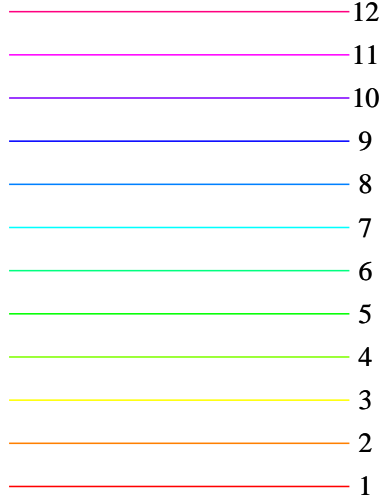


Figure 15: Colors of different levels in plots.

L	E_{tot}	E_{kin}	W_{00}	W_{XX}
1	1.17115	0.828479	0.641335	0.641335
2	1.12004	0.77663	0.665624	-2.33899
3	1.12209	0.767249	0.652168	-2.62701
4	1.10045	0.754992	0.659607	-1.11941
5	1.09696	0.750709	0.655268	-1.03139
6	1.08768	0.744818	0.652912	-1.7654
7	1.08567	0.740952	0.649266	-1.76564
8	1.0805	0.737844	0.649236	-1.24035
9	1.07929	0.735213	0.646753	-1.21667
10	1.07597	0.732495	0.644782	-1.54666
11	1.07518	0.73124	0.643665	-1.54135
12	1.07286	0.729149	0.642705	-1.27262

Table 3: The energy and the gauge-invariant observables of solutions constructed exactly at λ_{crit} for each given level.

References

- [1] E. Witten, “Noncommutative Geometry and String Field Theory,” Nucl. Phys. B **268**, 253 (1986).
- [2] M. Schnabl, “Analytic solution for tachyon condensation in open string field theory,” Adv. Theor. Math. Phys. **10**, 433 (2006) [hep-th/0511286].
- [3] M. Schnabl, “Comments on marginal deformations in open string field theory,” Phys. Lett. B

- 654**, 194 (2007) [hep-th/0701248].
- [4] M. Kiermaier, Y. Okawa, L. Rastelli and B. Zwiebach, “Analytic solutions for marginal deformations in open string field theory,” JHEP **0801**, 028 (2008) [hep-th/0701249].
 - [5] T. Erler, “Marginal Solutions for the Superstring,” JHEP **0707**, 050 (2007) [arXiv:0704.0930 [hep-th]].
 - [6] Y. Okawa, “Analytic solutions for marginal deformations in open superstring field theory,” JHEP **0709**, 084 (2007) [arXiv:0704.0936 [hep-th]].
 - [7] E. Fuchs, M. Kroyter and R. Potting, “Marginal deformations in string field theory,” JHEP **0709**, 101 (2007) [arXiv:0704.2222 [hep-th]].
 - [8] Y. Okawa, “Real analytic solutions for marginal deformations in open superstring field theory,” JHEP **0709**, 082 (2007) [arXiv:0704.3612 [hep-th]].
 - [9] I. Ellwood, “Rolling to the tachyon vacuum in string field theory,” JHEP **0712**, 028 (2007) [arXiv:0705.0013 [hep-th]].
 - [10] I. Kishimoto and Y. Michishita, “Comments on solutions for nonsingular currents in open string field theories,” Prog. Theor. Phys. **118**, 347 (2007) [arXiv:0706.0409 [hep-th]].
 - [11] E. Fuchs and M. Kroyter, “Marginal deformation for the photon in superstring field theory,” JHEP **0711**, 005 (2007) [arXiv:0706.0717 [hep-th]].
 - [12] M. Kiermaier and Y. Okawa, “Exact marginality in open string field theory: a general framework,” JHEP **0911**, 041 (2009) [arXiv:0707.4472 [hep-th]].
 - [13] M. Kiermaier and Y. Okawa, “General marginal deformations in open superstring field theory,” JHEP **0911**, 042 (2009) [arXiv:0708.3394 [hep-th]].
 - [14] O. K. Kwon, “Marginally Deformed Rolling Tachyon around the Tachyon Vacuum in Open String Field Theory,” Nucl. Phys. B **804**, 1 (2008) [arXiv:0801.0573 [hep-th]].
 - [15] S. Hellerman and M. Schnabl, “Light-like tachyon condensation in Open String Field Theory,” arXiv:0803.1184 [hep-th].
 - [16] I. Kishimoto, “Comments on gauge invariant overlaps for marginal solutions in open string field theory,” Prog. Theor. Phys. **120**, 875 (2008) [arXiv:0808.0355 [hep-th]].
 - [17] N. Barnaby, D. J. Mulryne, N. J. Nunes and P. Robinson, “Dynamics and Stability of Light-Like Tachyon Condensation,” JHEP **0903**, 018 (2009) [arXiv:0811.0608 [hep-th]].
 - [18] I. Ellwood, “Singular gauge transformations in string field theory,” JHEP **0905**, 037 (2009) [arXiv:0903.0390 [hep-th]].
 - [19] F. Beaujean and N. Moeller, “Delays in Open String Field Theory,” arXiv:0912.1232 [hep-th].
 - [20] M. Kiermaier, Y. Okawa and P. Soler, “Solutions from boundary condition changing operators in open string field theory,” JHEP **1103**, 122 (2011) [arXiv:1009.6185 [hep-th]].

- [21] T. Noumi and Y. Okawa, “Solutions from boundary condition changing operators in open superstring field theory,” *JHEP* **1112**, 034 (2011) [arXiv:1108.5317 [hep-th]].
- [22] A. Sen and B. Zwiebach, “Large marginal deformations in string field theory,” *JHEP* **0010**, 009 (2000) [hep-th/0007153].
- [23] A. Sen, “Energy momentum tensor and marginal deformations in open string field theory,” *JHEP* **0408**, 034 (2004) [hep-th/0403200].
- [24] A. Kurs, “Classical Solutions in String Field Theory,” Senior Thesis at Princeton University (2005).
- [25] A. Hashimoto and N. Itzhaki, “Observables of string field theory,” *JHEP* **0201**, 028 (2002) [hep-th/0111092].
- [26] D. Gaiotto, L. Rastelli, A. Sen and B. Zwiebach, “Ghost structure and closed strings in vacuum string field theory,” *Adv. Theor. Math. Phys.* **6**, 403 (2003) [hep-th/0111129].
- [27] I. Ellwood, “The Closed string tadpole in open string field theory,” *JHEP* **0808**, 063 (2008) [arXiv:0804.1131 [hep-th]].
- [28] N. Berkovits and M. Schnabl, “Yang-Mills action from open superstring field theory,” *JHEP* **0309**, 022 (2003) [hep-th/0307019].
- [29] T. Kawano, I. Kishimoto and T. Takahashi, “Gauge Invariant Overlaps for Classical Solutions in Open String Field Theory,” *Nucl. Phys. B* **803**, 135 (2008) [arXiv:0804.1541 [hep-th]].
- [30] A. Recknagel and V. Schomerus, “Boundary deformation theory and moduli spaces of D-branes,” *Nucl. Phys. B* **545**, 233 (1999) [hep-th/9811237].
- [31] A. Sen, “Rolling tachyon,” *JHEP* **0204**, 048 (2002) [hep-th/0203211].
- [32] L. Rastelli and B. Zwiebach, “Tachyon potentials, star products and universality,” *JHEP* **0109**, 038 (2001) [hep-th/0006240].
- [33] J. L. Karczmarek and M. Longton, “SFT on separated D-branes and D-brane translation,” *JHEP* **1208**, 057 (2012) [arXiv:1203.3805 [hep-th]].
- [34] M. Longton, “SFT Action for Separated D-branes,” arXiv:1203.4615 [hep-th].
- [35] M. Kiermaier, Y. Okawa and B. Zwiebach, “The boundary state from open string fields,” arXiv:0810.1737 [hep-th].
- [36] M. Kudrna, C. Maccaferri and M. Schnabl, “Boundary State from Ellwood Invariants,” arXiv:1207.4785 [hep-th].